TRENDS IN SCIENCES 2026; 23(3): 11834
https://doi.org/10.48048/tis.2026.11834 RESEARCH ARTICLE

Synthesis, Characterization, and Biogas Storage Performance of CO_2-Doped Petung Bamboo Activated Carbon

Dewa Ngakan Ketut Putra Negara[1,2,*], Made Sucipta[1], Tjokorda Gede Tirta Nindhia[1], I Made Gatot Karohika[1,2], I Gusti Komang Dwijana[1], I Gusti Agung Kade Suriadi[3], I Wayan Ryan Arta Wibawa[1] and Dewa Gede Arisma Dianata[1]

[1]Department of Mechanical Engineering, Udayana University, Bali 80361, Indonesia
[2]Master of Mechanical Engineering Study Program, Faculty of Engineering, Udayana University, Denpasar Bali 80114, Indonesia
[3]Department of Industrial Engineering, Udayana University, Bali 80361, Indonesia

([*]Corresponding author's e-mail: devputranegara@unud.ac.id)

Received: 9 September 2025, Revised: 29 September 2025, Accepted: 6 October 2025, Published: 15 December 2025

Abstract

The declining availability of fossil fuels requires the exploration of alternative renewable energy sources, such as biogas. The primary challenge associated with biogas utilization is storage. Traditional methods, such as compressed natural gas (CNG) and liquefied petroleum gas (LPG), require high pressures and very low temperatures, respectively, which reduce their overall efficiency. However, adsorbed natural gas (ANG) technology offers a better storage solution at low pressures by using adsorbent materials, including activated carbon. According to the results, there is limited research on using bamboo as a raw material for activated carbon in biogas storage. There is also limited information about how carbonization temperature affects pore structure, functional groups, and storage performance. Therefore, this research focuses on producing activated carbon from petung bamboo, characterizing the properties, and testing the effectiveness for biogas storage. Activated carbon is produced by carbonizing the bamboo at a temperature of 600 to 750 °C and activating it using CO_2. The results show that carbonization temperature influences pore structure, functional groups, and biogas storage capacity. Activated carbon carbonized at 750 °C (AC-750) shows the best performance based on proximate analysis, pore distribution, surface area, pore volume, and biogas adsorption capacity. AC-750 contains a strong C=C aromatic functional group and has a pore distribution that includes micro, meso, and macro pores. It has a surface area of 192.8 m^2/g, pore volume of 0.39 cc/g, and can store biogas up to 1.0 g/g at a pressure of 100 psi. Biogas release efficiency reached 92.9%, highlighting the potential of activated carbon made from petung bamboo for ANG applications. This result is significant as it highlights the potential of using abundant biomass resources as eco-friendly energy storage materials, thereby supporting sustainable energy security and facilitating the transition toward renewable energy.

Keywords: Activated carbon, Biogas, Carbonization temperature, Bamboo, Pore structure, Functional groups, Efficiency

Introduction

Energy has become a critical global strategic concern, drawing significant attention from nations worldwide. The demand for energy continues to rise annually, driven by factors such as population growth, industrialization, and improved living standards [1]. This condition creates a major challenge in providing sustainable, reliable, and affordable energy. The dependence on fossil energy sources such as petroleum, natural gas (NG), and coal is increasingly concerning, considering their dwindling reserves, while the exploration and production processes cause significant environmental impacts. In addition, the combustion of

fossil fuels is one of the main contributors to greenhouse gas emissions, which contribute to global warming and climate change [2,3].

In line with the results above, the development of environmentally friendly and renewable alternative energy has become a very urgent need. One renewable energy source that has enormous potential is biogas. Subsequently, biogas and NG are both gas fuels dominated by methane (CH_4) components, but with different concentrations. Biogas contains approximately 55% - 70% CH_4 by volume [4], while NG has a higher methane purity of approximately 97% by volume [5]. Biogas can be obtained through the anaerobic decomposition process of organic materials, such as agricultural waste, livestock manure, food waste, and other organic waste [6,7]. The advantages of biogas lie not only in the ability to produce energy but also in the environmental benefits, where the production process can reduce the volume of organic waste, suppress greenhouse gas emissions, and reduce dependence on fossil energy sources [6]. Thereby, biogas plays an important role as a renewable energy solution as well as a sustainable waste management strategy.

Despite its enormous potential, the optimal utilization of biogas continues to face several technical challenges, particularly in storage and distribution methods. Similar to natural gas, biogas needs to be stored under specific conditions to be used efficiently and safely. Commonly used gas storage technologies, such as Liquefied Natural Gas (LNG) and Compressed Natural Gas (CNG), have significant limitations. LNG requires very low temperatures (approximately –160 °C), requiring expensive cryogenic infrastructure and high energy consumption [8]. Meanwhile, CNG requires very high operating pressures (200-300 bar) [9], which poses a risk of leaks and explosions and requires special, heavy, and expensive pressurised tanks. These challenges have driven the search for safer, more energy-efficient, and more economical storage alternatives. A promising technology is Adsorbed Natural Gas (ANG), which uses porous materials such as activated carbon to adsorb methane molecules at much lower pressures, namely 35 - 70 bar [10]. This technology has the potential to reduce the cost of infrastructure, improve safety, and open up opportunities for wider biogas utilization in various sectors.

The success of an ANG system depends heavily on the type and quality of the adsorbent material used and the thermal management during the adsorption-desorption cycle [11,12]. Activated carbon (AC) is one of the most widely used materials in this application due to the high surface area, large micropore volume, good thermal and chemical stability [4,13,14], and abundant raw material availability. These properties enable activated carbon to effectively adsorb methane molecules through van der Waals forces [15], thereby increasing the gas storage capacity at low pressures. The characteristics of activated carbon, such as pore size distribution, specific surface area, and surface chemistry, can be controlled through the selection of raw materials and manufacturing process parameters.

Activated carbon raw materials can be derived from coal and petroleum residues [16]. However, due to the non-renewable nature and decreasing availability, alternative raw materials from biomass are very promising. One potential raw material is petung bamboo (Dendrocalamus asper), which is abundant, renewable, and rich in carbon, cellulose, and lignin [17]. Compared to other precursors such as coal and coconut shell, bamboo-derived activated carbon offers economic and environmental advantages. Bamboo is cheap and grows quickly, making it a sustainable and affordable choice for producing carbon. It also grows without the need for fertilizers or pesticides, which is better for the environment. On the other hand, coal-based activated carbon depends on fossil fuel extraction, which increases carbon emissions and harms the environment. Coconut shell is renewable and often considered more sustainable than coal, but bamboo's rapid growth and high biomass yield make it an even more eco-friendly option overall. Meanwhile, activated carbon is produced through the stages of dehydration, carbonization, and activation. Dehydration is carried out to remove water content from the raw material by preheating at low temperatures (approximately 220 °C) [18] without damaging the carbon structure. Carbonization is the main stage that converts organic material into a carbon framework and forms pore structure [19,20]. Temperature is one of the important parameters in the carbonization process [21-24] because it affects pore structure and surface area of the activated carbon produced [25]. At higher temperatures, the formation of additional micropores and larger mesopores enhances

adsorption capacity, which is particularly important in applications such as ANG storage and heavy metal adsorption. However, excessively high or uncontrolled temperatures may reduce the surface area, as the pore structure of the material can become damaged or degraded [26].

In the activation stage, new pores develop, existing pores widen, and pores that are still closed by carbonization products are opened [27]. At this stage, the activating gas, specifically physical activation, plays an important role in opening and expanding the carbon pore network, thereby increasing the surface area and pore volume, which are very much needed for adsorption applications, including ANG. Some frequently used activating gases are N_2 [28,29] and CO_2 [30,31]. Activation with CO_2 promotes the development of a high surface area and pore volume, thereby significantly enhancing the methane adsorption capacity [32]. Therefore, optimal carbonization temperature settings and the use of CO_2 activators are very necessary to produce activated carbon with a good balance of porosity and structural stability.

There is limited research on the use of bamboo as a source material for activated carbon in biogas storage. There is particularly little information on how carbonization temperature affects pore structure, functional groups, and biogas storage capacity. This study addresses this gap by investigating petung bamboo activated with CO_2 for Adsorbed Natural Gas applications. The objective is to investigate the influence of carbonization temperature on the quality of activated carbon for enhancing biogas storage capacity in an environmentally sustainable way.

Materials and methods

Materials and activated carbons production

As a precursor, petung bamboo from Baturiti Village, Tabanan, Bali, Indonesia, was used. According to earlier investigations, petung bamboo is composed of 19.35% hemicellulose, 28.69% lignin, and 37.33% cellulose [17]. Petung bamboo was sliced into ± 2×1×1 cm^3 pieces, cleaned with distilled water, allowed to dry in the sun for 5 days, and then dried in an electric furnace for 2 h at 105 °C. Furthermore, the dehydrated bamboo was carbonized at different temperatures of 600, 650, 700, and 750 °C at a rate of 10 °C per min [33], maintained there for 50 min, and then cooled for 12 h in an electric furnace. Selection of the carbonization temperature (600 - 750 °C) follows common practice for biomass-derived carbons, where major devolatilization is completed near 600 °C [34] and further heating up to 750 °C promotes bamboo activated carbon with acceptable quality [35]. Carbonized charcoal was ground into a powder, sieved using a 60-mesh, and entered into an activation reactor ready to be activated. With a CO_2 activator flowing at 300 mL/min, controlled by a flowrate controller, the activation process was carried out by heating to 750 °C at a rate of 10 °C/min, held for 50 min, and then cooled to room temperature inside the furnace [36]. The generated activated carbon was put in an airtight plastic bottle after cooling to room temperature in an electric furnace.

Activated carbon characterization

To obtain detailed information on the chemical and physical characteristics of activated carbon, characteristic tests were carried out. To ascertain the amount of ash, moisture, fixed carbon, and volatile carbon in activated carbon, a TGA test was first performed using a TGA 701 ASTM D7582 MVA in Coal instrument. Pore surface area, pore volume, pore diameter, and pore size distribution of the activated carbon material were then measured using an adsorption isotherm test with a SAA Analyser Quantachrome NovaWin Version 11.0. Additionally, an FTIR test was performed using a Shimadzu IR Prestige-21 FTIR instrument to identify functional groups contained in activated carbon, and a SEM test was performed using a JSM-6510LA SEM instrument to evaluate the surface morphology of activated carbon. Lastly, the degree of crystallinity and crystal size of activated carbon were assessed using an XRD test using PANalytical X'Pert PRO.

Biogas storage tests

Using the test scheme shown in **Figure 1**, biogas was stored using the gravimetric approach, which calculates storage capacity based on changes in mass [37,38]. First, the scale of digital balance was set to zero. Next, 50 g of AC-600 activated carbon was added to the tube (biogas storage cylinder), and the tube was suctioned until the pressure dropped to −30 psi. The tube containing the activated carbon was weighed, and the compressor was started to move biogas from the plastic

store (biogas storage bag) to the tube at variation pressures between 0 and 100 psi. The tube valve was closed after the pressure was attained, and the filling time at each pressure, as well as the mass readings on the scale, were meticulously reported. Furthermore, biogas was gradually released from the tube during the desorption process, and when the pressure dropped from 100 to 0 psi, the scale readings and biogas release time were reported. To guarantee data consistency, the full adsorption and desorption procedure was carried out 3 times. Comparable procedures were also used to test activated carbon types AC-650 through AC-750. The mass difference between the activated carbon tube before and after biogas storage was used to determine biogas storage capacity at each pressure.

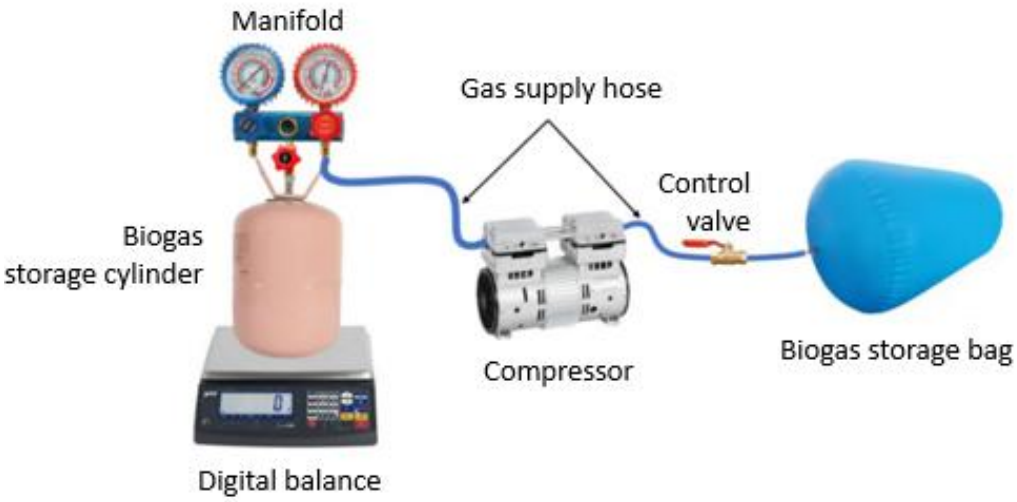

Figure 1 The scheme of biogas storage.

Results and discussion

TGA composition analysis of activated carbon

According to Thermogravimetric Analysis (TGA), as shown in **Table 1**, the levels of moisture, volatile matter, and ash fluctuate. At the same time, the fixed carbon content gradually increases as the temperature rises. Generally, the quality of activated carbon improves with rising temperatures [39]. This indicates that carbonization temperature has a crucial role in the proximate characteristic of activated carbon. The fixed carbon content increased from about 69% in the 600 to 700 °C range to approximately 74% at 750 °C. This change shows a more complete carbonization process and a stronger carbon structure. The volatile matter content stayed relatively stable at around 12% between 600 and 700 °C, but fell to about 10% at 750 °C. This drop shows a more thorough devolatilization process. Additionally, the ash content was quite high at 600 to 700 °C, approximately 9%, but dropped significantly to roughly 6% at 750 °C. This suggests a reduction in mineral residues or the impact of burn-off during the activation phase. Activated carbon with a high fixed carbon content and low levels of volatile matter, moisture, and ash is preferred for adsorption applications. This specification is important because it improves thermal stability, increases surface area, and enhances absorption efficiency [40].

The results from the TGA composition show that all samples met the Indonesian National Standard (SNI 06-3730-1995) for powder AC. This standard states that powdered activated carbon should not have a volatile matter content above 25%, a moisture content above 15%, or an ash content above 10%, while maintaining a minimum fixed carbon content of 65% [40]. In general, the composition analysis shows that AC-750 activated carbon has the highest fixed carbon content and the lowest levels of volatiles and ash. These favorable properties are strongly influenced by the activation process; in particular, activating carbon at high temperatures with CO_2 helps create and expand pores through the reaction $C + CO_2 \rightarrow 2CO$, which is key for increasing surface area [41].

Table 1 Proximate composition of AC materials.

Sampel	Moisture (%)	Volatile (%)	Ash (%)	Fix carbon (%)
AC-600	10.1	11.92	8.96	69.02
AC-650	9.86	12.08	8.53	69.53
AC-700	9.96	12.26	9.90	69.88
AC-750	9.97	10.07	5.99	73.97

FTIR and XRD analysis

Based on the FTIR spectra results of activated carbon at different carbonization temperatures (AC-600, AC-650, AC-700 and AC-750), as shown in **Figure 2**, the 4 samples showed similar main functional groups. These include hydroxyl O-H stretching (around 3,400 cm^{-1}) [42] and 3,568 cm^{-1} [43], aliphatic C-H (2,920 - 2,850 cm^{-1}) [42,44], carbonyl group C=O (~1,700 cm^{-1}) [44], aromatic vibration C=C (~1,600 cm^{-1}) [44], and phenols and ethers C-O bands at 1,200 - 1,050 cm^{-1} [45]. This similarity shows that all activated carbon still contains functional oxygen groups such as hydroxyl, carboxyl, phenolic, and ether, though the intensity varies with carbonization temperature. Generally, raising the carbonization temperature from 600 to 750 °C leads to a decrease in the intensity of the oxygen group bands (O-H, C=O and C-O) and aliphatic C-H. At the same time, the aromatic C=C bands become more prominent. This trend suggests a gradual deoxygenation process and an increase in the aromatic and graphitic properties on the activated carbon surface. As a result, the surface properties shift from more polar and hydrophilic (AC-600) to more hydrophobic and aromatic (AC-750) [46].

Oxygen-containing functional groups play an important role in determining the selective adsorption of CO_2 and CH_4 in biogas. The reduction of oxygen-containing functional groups at higher carbonization temperatures lowers the number of polar adsorption sites. This weakens CO_2 affinity and slows its adsorption and desorption kinetics. Since CH_4 is nonpolar and has a larger kinetic diameter, its uptake is less influenced by surface features. It is mainly determined by pore structure. Consequently, CO_2 selectivity typically decreases when oxygen groups are reduced, while CH_4 adsorption behavior stays relatively stable [47].

The XRD pattern of activated carbon carbonized at different temperatures (600 - 750 °C), as seen in **Figure 3**, shows a broad and unclear peak in the 2θ range around 20° - 30°, and a weak shoulder near approximately 42° - 45°. This is typical for amorphous carbon materials with small graphitic domains. The 2θ peaks approximately 23° - 25° and 43° [48], as well as 25° - 25° and 43° - 44° [49], are also reported as diffraction patterns that characterize amorphous activated carbon. At 600 °C, the diffraction pattern remains very broad with relatively high intensity, showing the dominance of the amorphous phase. As the temperature rises to 650 - 700 °C, the peaks become a bit more defined, showing some formation of graphitic structural ordering, though still on a limited scale. This suggests a trend towards increased crystallinity due to the rearrangement of carbon layers. However, at 750 °C, the relative intensity decreases, and peak broadening is still evident. This shows that further temperature increases do not significantly enhance crystallinity. Therefore, the XRD results confirm that activated carbon mostly stays amorphous, with minor increases in crystallinity between 650 - 700 °C, while higher temperatures may disrupt the structural organization, leaving it mainly made up of amorphous structures.

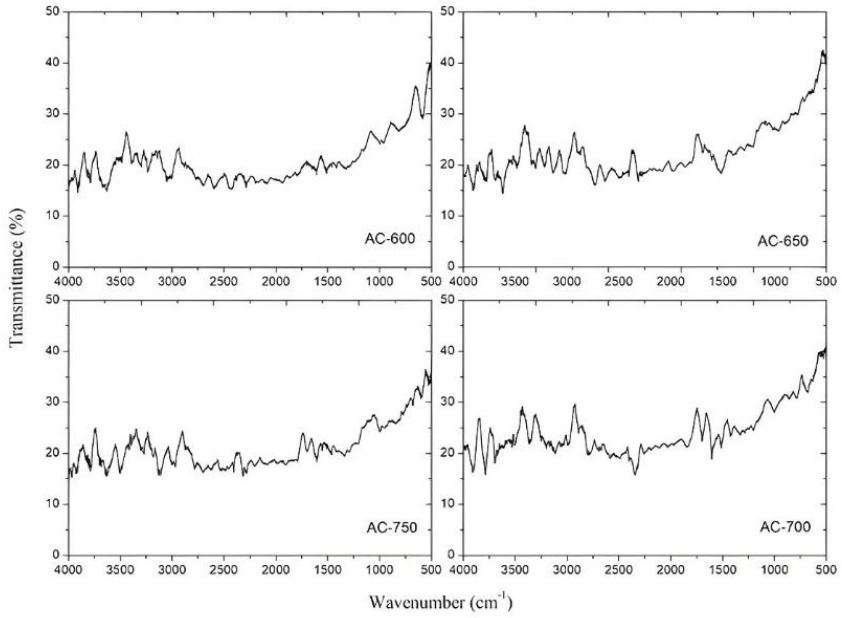

Figure 2 FTIR analysis of activated carbons.

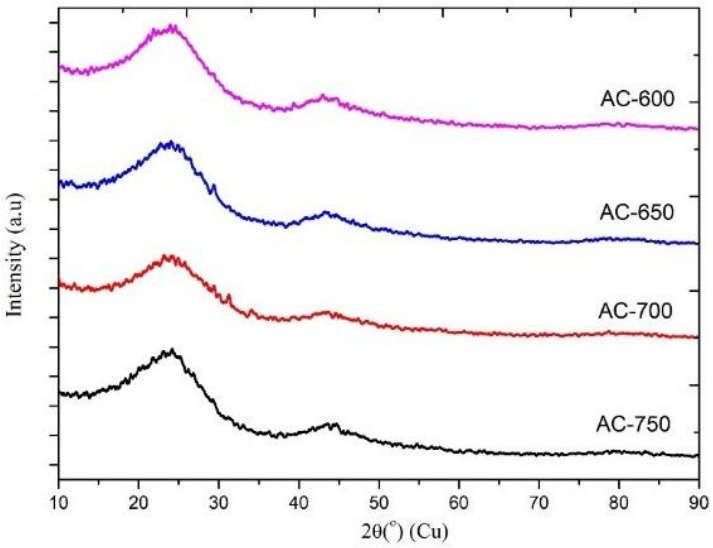

Figure 3 XRD patterns of activated carbons.

SEM analysis

The carbonization process at different temperatures greatly affects pore formation and development, which in turn influences the final properties of the material. SEM (Scanning Electron Microscopy) observations, shown in **Figure 4**, show the surface structure of activated carbon created at carbonization temperatures of 600, 650, 700, and 750 °C. At 600 °C, pores remain relatively small, partially closed, and largely isolated. However, at 650 °C, the number of pores increases and their size begins to grow. By 700 °C, the structure is more developed with relatively uniform pores and good connectivity between them, suggesting a potential for a larger surface area. At 750 °C, pores become larger and more interconnected, with thinner walls separating them. In general, raising carbonization temperature leads to an increase in both the size and number of pores, but excessive temperatures may risk reducing structural stability.

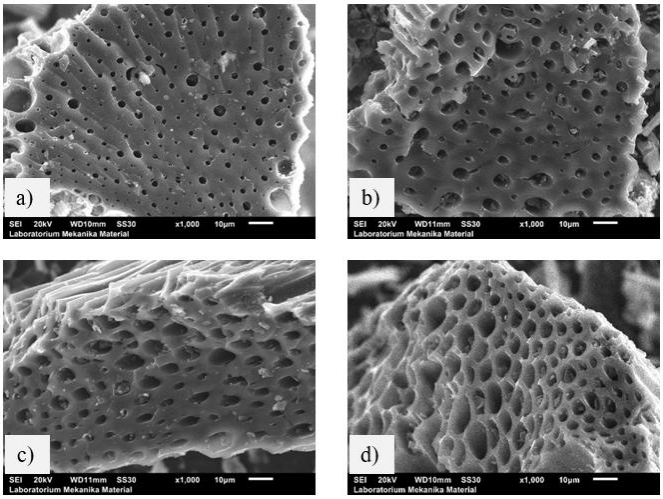

Figure 4 SEM images of activated carbon samples: (a) Ac-600, (b) AC-650, (c) AC-700 and (d) AC-750.

Adsorption isotherm of AC

Four adsorption isotherm curves of activated carbon samples with different carbonization temperatures, AC-600, AC-650, AC-700, and AC-750, are shown in **Figure 5**. The graphs show type IV (IUPAC), which is typical for mesoporous materials. There is a significant rise in adsorption at high P/P_0, showing capillary condensation in the mesopores [50]. The differences between the curves highlight the effect of carbonization temperature on adsorption capacity and pore volume. As the carbonization temperature increases, the nitrogen adsorption capacity also rises. This relates to the development of micropores and the surface area of activated carbon, which grows with temperature, as confirmed from pore structure, as shown in **Table 4**.

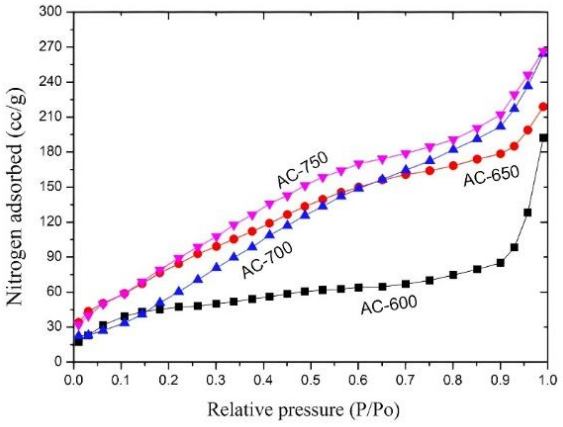

Figure 5 Adsorption isotherm of activated carbon.

In AC-600, the amount of nitrogen adsorbed was the lowest across all pressure levels. This matches its low specific surface area and pore volume, as shown by the surface structure data in **Table 4** and the cumulative pore volume in **Figure 6(b)**. This shows that AC-600 has a restricted pore structure, leading to a low adsorption capacity. AC-650 showed a notable improvement compared to AC-600, which had a higher isotherm curve throughout the pressure range, corresponding to an increase in specific surface area (126.28 m^2/g) and pore volume (0.306 cc/g). In AC-700, the nitrogen adsorption was even higher, particularly at low to medium pressures, which suggests that small micropores are more prominent than small mesopores.

This result is in line with pore distribution peaking approximately 3 nm in diameter, and the SEM images showing dense and uniform pores. Meanwhile, AC-750 exhibited the highest nitrogen adsorption capacity across the relative pressure range. This suggests that this activated carbon features a large surface area (192.77 m^2/g) and the greatest pore volume (0.390 cc/g). A significant increase in adsorption at medium to high pressures shows that mesopores play a larger role. This is consistent with pore size distribution results, which show the presence of large pores (> 2 nm) due to either pore enlargement or coalescence at higher carbonization temperatures.

Adsorption at low P/P_0 (< 0.1) points to micropores [51]. AC-750 exhibited the highest initial adsorption, showing many micropores. Adsorption at high P/P_0 (> 0.8) suggests macropores [52]. All samples experienced a sharp increase, but AC-750 and AC-700 were more prominent, showing a mix of micro- and meso/macropores.

Pore size and surface area distribution

The graph in **Figure 6** shows pore size distribution and cumulative pore volume of activated carbon samples (AC-600, AC-650, AC-700 and AC-750). Pore size distribution shows that microscopic pores in the 1 - 2 nm and mesopore range (2 - 6 nm) dominate in all samples. AC-750 has an extra mesoporous peak at around 26 - 27 nm, and this peak is more significant than in the other samples. The cumulative pore volume increases with pore size. AC-750 and AC-700 have a greater total porosity than AC-600 and AC-650, which means they have a higher pore storage capacity.

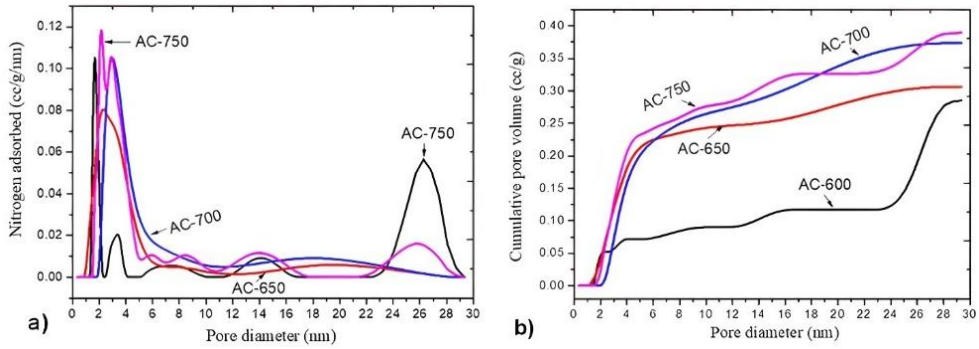

Figure 6 (a) Pore size distribution and (b) Cumulative pore volume.

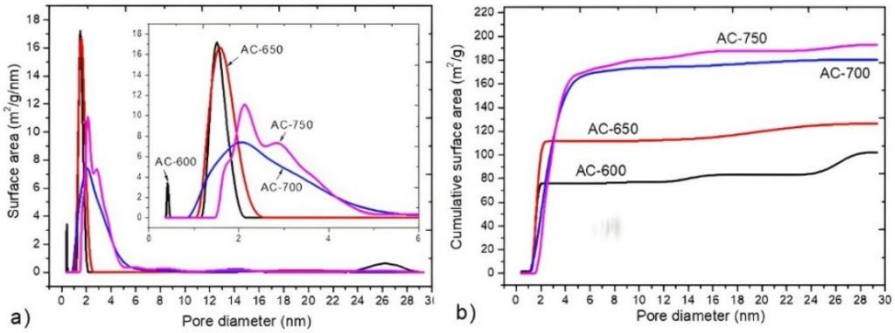

Figure 7 (a) Surface area distribution and (b) cumulative surface area.

In **Figure 7**, the surface area distribution and cumulative surface area show that micropores contribute the most to the surface area in all samples. AC-750 also exhibits a strong distribution within the mesopore region, resulting in the largest overall surface area. This is followed by AC-700, AC-650, and AC-600, as shown in **Table 4**, which suggests that AC-750 offers more active surface area for adsorption. The rise in cumulative surface area with pore diameter shows that samples activated at higher temperatures (AC-750, AC-

700) have a mix of micropores and mesopores that enhance adsorption performance compared to samples activated at lower temperatures. **Table 4** (surface structure of activated carbon) confirms this trend, as increasing carbonization temperature leads to a larger surface area and pore volume in activated carbon.

Table 4 Surface structure of activated carbons.

Samples	Surface structure		
	S_{BET} (m^2/g)	V_P (cc/g)	D_P (nm)
AC-600	102.212	0.285	4.804
AC-650	126.288	0.306	3.358
AC-700	180.450	0.374	3.051
AC-750	192.771	0.390	4.177

Biogas storage

Figure 8 shows a graph of biogas adsorption and desorption on carbonized activated carbon at temperatures of 600, 650, 700, and 750 °C. There is a clear link between rising pressure and biogas adsorption and desorption capacity. In the adsorption process (**Figure 8(a)**), increasing pressure from 0 to 100 psi consistently raises the amount of biogas adsorbed by activated carbon. This means that higher pressure pushes biogas molecules more strongly to stick to the surface and enter pores of the activated carbon, significantly increasing its biogas storage capacity [53]. For activated carbon carbonized at 750 °C (AC-750), this capacity increase is most notable, reaching almost 1.011 g/g at the highest pressure. On the other hand, in the desorption process (**Figure 8(b)**), lowering the pressure from 100 to 0 psi leads to the release of biogas stored in the activated carbon. Biogas release is greater for activated carbon with a higher carbonization temperature, specifically AC-750, which shows good release capacity as pressure drops. This relationship shows that pressure changes are crucial in biogas adsorption and desorption processes on activated carbon; high pressure encourages biogas adsorption, and low-pressure aids in biogas release. Therefore, activated carbon-based biogas storage systems depend on cycles of pressure change for effective storage and release of biogas [29].

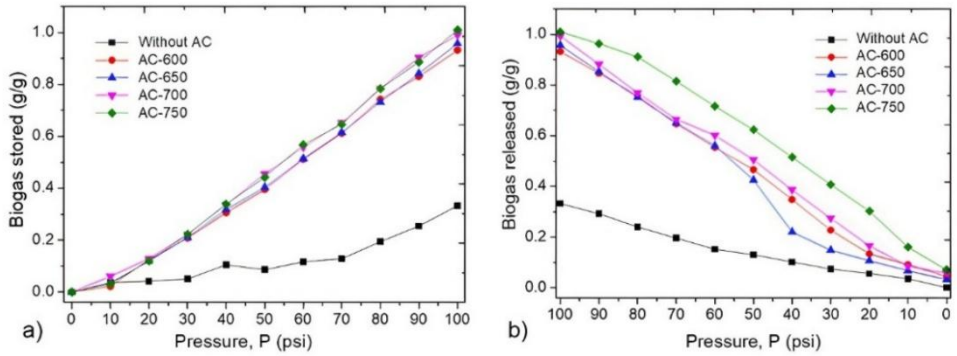

Figure 8 (a) Biogas adsorption and (b) biogas desorption.

Figure 9 shows the maximum storage capacity of activated carbon at 100 psi, the release capacity at 0 psi, and the remaining biogas capacity of activated carbon. Using activated carbon has been shown to improve storage capacity compared to without activated carbon. Biogas storage increases reached 64.377%, 65.308%, 66.565%, and 67.161% for activated carbon AC-600, AC-650, AC-700, and AC-750, respectively. AC-600 stored and released the lowest amount of biogas due to its small surface area and limited pores. Higher carbonization temperatures led to better performance, as seen in AC-650 (0.957 g/g) and AC-700 (0.993 g/g). These types have a dominant micropore and small mesopore distribution that supports efficient gas

adsorption and release. AC-750 achieved the highest storage capacity at 1.011 g/g, which is in line with the larger surface area and pore volume. However, some gas remained trapped in the larger pores, making the release efficiency only 92.97%. Nevertheless, its efficiency is still higher compared to other activated carbons.

When biogas was stored without activated carbon, it was completely released. In contrast, when stored with activated carbon, a portion of biogas remained adsorbed within the material, showing its capacity to retain gas molecules. This relates to the characteristics of activated carbon and the adsorption process. CH_4 molecules that adsorb on the surface and in pores of activated carbon connect through Van der Waals forces [15,54]. Some of these molecules become tightly confined within the micropores and mesopores, making them difficult to release through simple changes in pressure or temperature. Additionally, activated carbon has a complex and varied pore structure, including very small micropores. Gas molecules caught in these narrow spaces can struggle to escape, which leads to some gas being trapped [29,53].

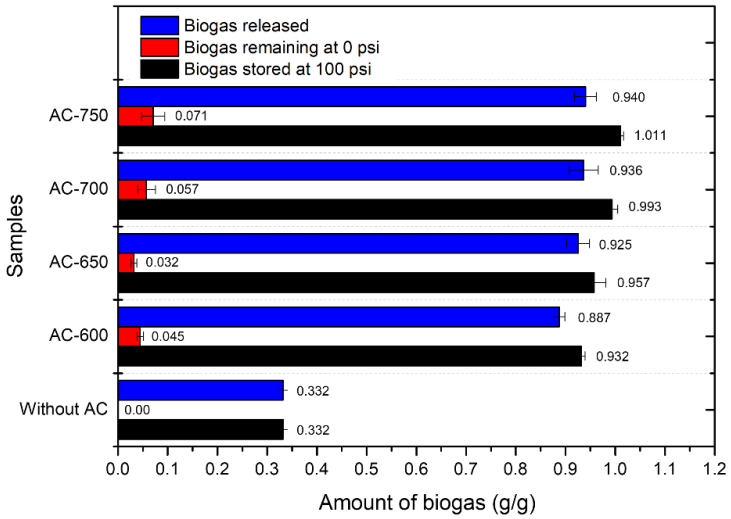

Figure 9 Stored, released, and residual biogas.

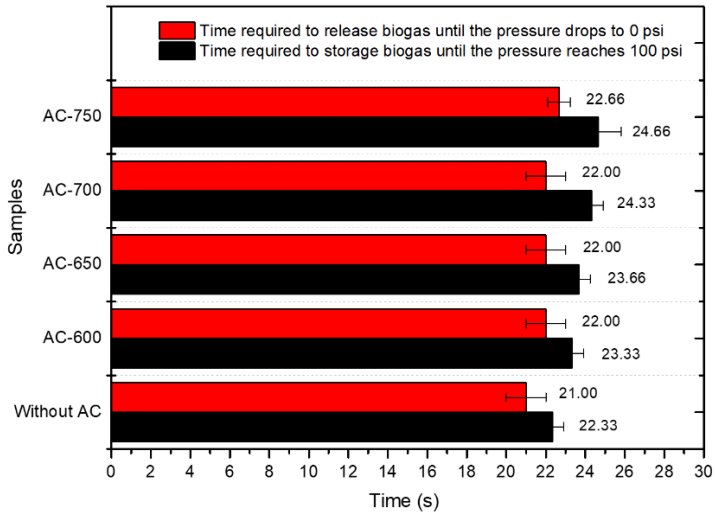

Figure 10 Time required for biogas storage and release.

Figure 10 shows the time needed for biogas storage at 100 psi and the time required to release biogas from 100 to 0 psi. The release time for biogas from activated carbon carbonized at 600 to 750 °C is fairly constant, approximately 22 to 22.66 s. AC-750 shows the longest release time, which shows a stronger bond of

biogas within its pores. In contrast, the time for biogas storage tends to increase with higher carbonization temperatures, going from about 22 s at AC-600 to 24.66 s at AC-750. This pattern relates to the structure of activated carbon. At low temperatures (600 °C), pores have not developed well, resulting in low storage capacity. At medium temperatures (650 °C), pores are more open and can hold biogas more effectively. At high temperatures (700 to 750 °C), pore development becomes more complex, and in some cases, narrowing occurs due to carbon sintering. High-temperature carbonization has also been reported to promote sintering in the pores of activated carbon [55]. This makes the gas filling process slower, even though the adsorption capacity increases.

Many ANG studies use 35-70 bar as a practical filling pressure [10]. For initial studies, the pressure range varies from 5 to 100 bar [56]. The pressures up to 100 psi (6.9 bar) in this study are still useful. They allow for comparisons between samples under relatively low filling conditions. This way, micro and micro-meso pore effects and kinetics can be applied without high thermal and pressure issues. Additionally, initial testing at lower pressures cuts down on the need for highly certified equipment and lowers safety risks when evaluating many samples. Although the operating pressure was lower than typical ANG targets, the observed trends are still meaningful when linked with pore structure characterization. In general, the connections between SEM, pore structure, nitrogen adsorption isotherms, and biogas storage tests reinforce each other. Higher carbonization temperatures increase the surface area and pore volume, which directly boost biogas adsorption and storage capacity. Therefore, the novelty of this research lies in the use of petung bamboo as an activated carbon precursor for ANG applications, which can produce adsorbents with a combination of multi-level pore distribution (micro, meso and macro), optimal surface area and pore volume, and high gas storage and release efficiency.

Conclusions

This research showed that carbonization temperature significantly affects the properties of activated carbon. Higher carbonization temperatures increase fixed carbon composition, reduce the oxygen group bands, and show the presence of C=C aromatic bands, particularly in AC-750. The reduction of oxygen-containing functional groups is helpful for improving CH_4 storage selectivity over CO_2. The adsorbent surface becomes less polar, making it more suitable for nonpolar gas molecules. In addition, the C=C aromatic functional group is good for adsorbing nonpolar molecules like CH_4, which is the main component of biogas. Beyond the influence of surface chemistry, the structural characteristics of AC-750 further contribute to its superior adsorption performance. Additionally, AC-750 has benefits in its structure, featuring more open and interconnected pores. Pore distribution spans from micropores to macropores, and it has the highest surface area and cumulative pore volume compared to the other samples. This allows AC-750 to store and release the largest amount of biogas. A limitation of this research is the lack of selectivity tests for individual biogas components, the absence of regeneration tests for activated carbon over multiple cycles, the reliance on a single synthesis batch, and the omission of tests for mechanical strength and attrition resistance. Future research should include multicomponent sorption tests, analysis of adsorption and desorption cycles, and surface modification strategies to improve the selectivity and stability of the adsorbent. It should also evaluate multiple batches from different bamboo sources to confirm the reproducibility and reliability of the performance of AC-750. Additionally, future studies should address the mechanical strength and attrition resistance, as these factors are important for ensuring the durability of activated carbon in practical ANG applications.

Acknowledgements

The author thanks the Directorate of Research, Technology, and Community Service (DRTPM) of the Ministry of Higher Education, Science, and Technology of the Republic of Indonesia for supporting this research under master contract 121/C3/DT.05.00/PL/2025. Similarly, the Institute for Research and Community Service at Udayana University facilitated this research through the derivative contract: B/335 42/UN14.4.A/PT.01.03/2025.

Declaration of Generative AI in Scientific Writing

The authors admit using generative AI technologies, such as Grammarly, and OpenAI's

ChatGPT, to produce this work, mostly for language editing and grammar correction. In addition, this article has been reviewed by native English speaker. No content generation or data interpretation was performed by AI. The authors take full responsibility for the content and conclusions of this work.

CRediT Author Statement

Dewa Ngakan Ketut Putra Negara: Conceptualization, Resources, Funding acquisition, and Writing - review & editing. **Made Sucipta**: Conceptualization, Methodology, Supervision, Validation, and Writing - original draft. **Tjokorda Gede Tirta Nindhia**: Data curation, Formal analysis, Investigation, Validation, and Visualization. **I Made Gatot Karohika**: Data curation, Formal analysis, Investigation, Validation, and Visualization. **I Gusti Komang Dwijana**: Data curation, Investigation, Validation, and Visualization. **I Gusti Agung Kade Suriadi**: Data curation, Investigation, Validation, and Visualization. **I Wayan Ryan Arta Wibawa**: Data curation, Investigation, Validation, and Visualization. **Dewa Gede Arisma Dianata**: Data curation, Investigation, Validation, and Visualization.

References

[1] L Cozzi and T Gould. World energy outlook 2023, International Energy Agency. Available at: https://www.iea.org/reports/world-energy-outlook-2023, accessed May 2025.

[2] H Lee, K Calvin, D Dasgupta, G Krinner, A Mukherji, P Thorne, C Trisos, J Romero, P Aldunce, K Barrett, G Blanco, WWL Cheung, SL Connors, F Denton, A Diongue-Niang, D Dodman, M Garschagen, O Geden, B Hayward, C Jones, F Jotzo, T Krug, R Lasco, JY Lee, V Masson-Delmotte , M Meinshausen, K Mintenbeck, A Mokssit, FEL Otto, M Pathak, A Pirani, E Poloczanska, HO Pörtner, A Revi, DC Roberts , J Roy , AC. Ruane , J Skea, PR Shukla , R Slade , A Slangen , Y Sokona , AA Sörensson , M Tignor, DV Vuuren, YM Wei, H Winkler, P Zhai, and Z Zommers. Climate Change 2023. AR6 Synthesis Report, DOI:10.59327/IPCC/AR6-9789291691647.001. Accessed May 2025.

[3] S Wolf, R Bullard, JJ Buonocore, N Donley, T Farrelly, J Fleming, DJX González, N Oreskes, W Ripple, R Saha and MD Willis. Scientists' warning on fossil fuels. *Oxford Open Climate Change* 2025; **5(1)**, 1-26.

[4] W Saadi, B Ruiz, S Najar-souissi, A Ouederni and E Fuente. High-pressure gas adsorption on activated carbons from pomegranate peels biochar: A promising approach for biogas purification. *Biomass and Bioenergy* 2024; **186**, 107258.

[5] E Surra, RPPL Ribeiro, T Santos, M Bernardo, JPB Mota, N Lapa and IAAC Esteves. Evaluation of activated carbons produced from maize cob waste for adsorption-based CO_2 separation and biogas upgrading. *Journal of Environmental Chemical Engineering* 2022; **10(1)**, 107065.

[6] A Alengebawy, Y Ran, AI Osman, K Jin, M Samer and P Ai. Anaerobic digestion of agricultural waste for biogas production and sustainable bioenergy recovery: A review. *Environmental Chemistry Letters* 2024; **22(6)**, 2641-2668.

[7] AH Ulukardesler. Anaerobic co-digestion of grass and cow manure: kinetic and GHG calculations. *Scientific Reports* 2023; **13(1)**, 6320.

[8] R Bruno, V Ferraro, A Cristaudo and P Bevilacqua. A novel system based on a series of ORCs to recover cryogenic energy from the LNG regasification process for power and freshwater production. *Journal of Cleaner Production* 2024; **469**, 14317.

[9] Y Ali, A Younus, A Ullah and AH Alrefai. Compressed Natural Gas (CNG) as a fuel and the associated risks: A quantitative analysis in the scenario of a developing country. *Journal of Safety Science and Resilience* 2024; **5(3)**, 306-316.

[10] AV Shkolin, EM Strizhenov, SS Chugaev, IE Men'shchikov, VV Gaidamavichute, AE Grinchenko and AA Zherdev. Natural gas storage filled with peat-derived carbon adsorbent : Influence of nonisothermal effects and ethane impurities on the storage cycle. *Nanomaterials* 2022; **12(22)**, 4066.

[11] IE Men, AV Shkolin, EM Strizhenov and AA Zherdev. Thermodynamic behaviors of adsorbed methane storage systems based on nanoporous carbon adsorbents prepared from coconut shells. *Nanomaterials* 2020; **10(11)**, 2243.

[12] EM Strizhenov, SS Chugaev, IE Men and AV Shkolin. Heat and mass transfer in an adsorbed natural gas storage system filled with monolithic carbon adsorbent during circulating gas charging. *Nanomaterials* 2021; **11(12)**, 3274.

[13] J Serafin, Ba Dziejarski, P Rodríguez-Estupiñán, VB Fernández, L Giraldo, J Sreńscek-Nazzal, B Michalkiewicz and JC Moreno-Piraján. Effective synthesis route of renewable activated biocarbons adsorbent for high CO_2, CH_4, H_2, N_2, C_2H_4 gas storage and CO_2/N_2, CO_2/CH_4, CO_2/H_2, C_2H_4/CH_4 selectivity. *Fuel* 2024; **374**, 132462.

[14] S Mirzaei, L Lotfikatooli, A Ahmadpour, M Niknam, M Reza and A Arami-niya. Enhancing energy carrier gas storage: Novel MOF-decorated carbons with high affinity toward methane and hydrogen. *Chemical Engineering Research and Design* 2024; **203**, 419-430.

[15] JH Lee, J Lee, D Kim, S Lee and S Park. Unveiling pore size contributions and host-guest interactions in methane adsorption under varying pressure conditions: A semi-empirical adsorption model. *NPG Asia Materials* 2025; **17(1)**, 30.

[16] MO Azeez and SA Ganiyu. Review of biomass derived-activated carbon for production of clean fuels by adsorptive desulfurization: Insights into processes, modifications, properties, and performances. *Arabian Journal of Chemistry* 2023; **16(10)**, 105182.

[17] DNKP Negara, TGT Nindhia, IM Widiyarta, IGK Dwijana, DGA Dinata, G Prasetiyo, IDMPH Wardana and IW RA Wibawa. Characteristics evaluation of 3 Balinese as precursor of activated carbon. *In*: Proceedings of the 7th International Conference on Materials Engineering and Nanotechnology 2023 (ICMEN 2023), Kuala Lumpur, Malaysia. 2023, p. 44-53.

[18] G Hyeon, GB Lee, DJ Kang, SE Lee, KM Seong and J Park. Optimization of activated carbon synthesis from spent coffee grounds for enhanced adsorption performance. *Molecules* 2025; **30(12)**, 2557.

[19] M Kwiatkowski. An analysis of textural properties of activated carbons obtained from biomass via the LBET, NLDFT and QSDFT methods. *Scientific Reports* 2024; **14(1)**, 26472.

[20] Q Wang, B Luo, Z Wang, Y Hu and M Du. Pore engineering in biogas-derived activated carbon materials for enhance energy, catalysis, and environmental applications. *Molecules* 2024; **29(21)**, 5172.

[21] H Feng, T Zhou, L Ge, Q Li, C Zhao, J Huang and Y Wang. Study on the preparation of high value-added activated carbon from petroleum coke: Comparison between 1-and 2-step methods for carbonization and activation. *Energy* 2024; **292**, 130570.

[22] C Quan, H Wang, X Jia and N Gao. Effect of carbonization temperature on CO_2 adsorption behavior of activated coal char. *Journal of the Energy Institute* 2021; **97**, 92-99.

[23] G Liu, C Zhang, D Dou and Y Wei. Modeling and optimization of activated carbon carbonization process based on support vector machine. *Physicochemical Problems of Mineral Processing* 2021; **57(2)**, 131-143.

[24] I Karume, S Bbumba, S Tewolde, IZT Mukasa and M Ntale. Impact of carbonization conditions and adsorbate nature on the performance of activated carbon in water treatment. *BMC Chemistry* 2023; **17(1)**, 1162.

[25] MS Hafizuddin, CL Lee, KL Chin, PS H'ng, PS Khoo and U Rashid. Fabrication of highly microporous structure activated carbon via surface modification with sodium hydroxide. *Polymer* 2021; **13(22)**, 3954.

[26] W Chi, G Wang, Z Qiu, Q Li, Z Xu, Z Li, B Qi, K Cao, C Chi, T Wei and Z Fan. Secondary high-temperature treatment of porous carbons for high-performance supercapacitors. *Batteries* 2024; **10(5)**, 1-12.

[27] A Pimsawat, A Tangtrakarn, N Pimsawat, A Khamkongkaeo and S Daengsakul. Microwave assisted activation of silkworm excrement for fast adsorption of methylene blue and high performance supercapacitor. *Scientific Reports* 2024; **14(1)**, 26868.

[28] TM Budnyak, IV Pylypchuk, ME Lindström and O Sevastyanova. Kraft lignin-derived microporous nitrogen-doped carbon adsorbent for air and water purification. *ACS Applied Materials & Interfaces* 2024; **16(3)**, 3427-3441.

[29] M Lotfinezhad, M Tahmasebpoor and C Pevida. Exploring the structural characteristics and adsorption capabilities of cost-effective N-doped activated carbon derived from waste biomass for CO_2 adsorption. *Environmental Research* 2024; **263**, 120017.

[30] Y Ye, W Chen, C Tsai and W Tsai. The combination of nitrogen (N_2) pyrolysis and carbon dioxide (CO_2) Activation for regenerating spent activated carbon. *Applied Sciences* 2025; **15(10)**, 5336.

[31] DNKP Negara, TGT Nindhia, IM Widiyarta, IMG Karohika, IMG Suarda and IGK Dwijana. Characteristics and performance analysis of activated carbons derived from different precursors and activators for waste water adsorption. *EUREKA: Physics and Engineering* 2023; **6**, 160-172.

[32] D Peredo-Mancilla, I Ghouma, C Hort, CM Ghimbeu, M Jeguirim and D Bessieres. CO_2 and CH_4 adsorption behavior of biomass-based activated carbons. *Energies* 2018; **11(11)**, 3136.

[33] DNKP Negara, TGT Nindhia, CIPK Kencanawati, IGAK Suriadi, IM Widiyarta, IP Lokantara and IN Budiarsa. The effect of carbonisation heating rates on the properties of N-doped teak sawdust waste activated carbon. *Journal of Physical Science* 2023; **34(3)**, 1-20.

[34] W Zhao, L Luo, H Wang and M Fan. Synthesis of bamboo-based activated carbons with super-high specific surface area for hydrogen storage. *BioResources* 2017; **12(1)**, 1246-1262.

[35] N Jarawi and I Jusoh. Charcoal properties of Malaysian bamboo charcoal carbonized at 750 °C. *Bioresources* 2023; **18(3)**, 4413-4429.

[36] IG Agung, DNKP Negara, TGT Nindhia, IKA Atmika, IMDB Penindra and IMG Karohika. The impact of activation heating rate on pore structure in teak sawdust-derived activated carbon and its application in methylene blue adsorption. *Trends in Sciences* 2024; **21(9)**, 8110.

[37] PAS Cavazos, E Hunter-sellars, P Iacomi, SR Mcintyre, D Danaci and DR Williams. Evaluating solid sorbents for CO_2 capture: Linking material properties and process efficiency via adsorption performance. *Frontiers in Energy Research* 2023; **11**, 1167043.

[38] D Obracaj, M Korzec and M Korzec. Comparison of gravimetric determination of methane sorption capacities of coals for using their results in assessing. *Energies* 2024; **17(17)**, 4372.

[39] R Kumar, B Singh and B Acharya. A comprehensive review on activated carbon from pyrolysis of lignocellulosic biomass: An application for energy and the environment. *Carbon Resources Conversion* 2024; **7(4)**, 100228.

[40] J Pramana, G Sutapa, G Lukmandaru and S Sunarta. Conversion of shoot waste of fast-growing teak into activated carbon and its adsorption properties. *Journal of the Korean Wood Science and Technology* 2024; **52(5)**, 488-503.

[41] C Quan, Y Zhou, J Wang, C Wu and N Gao. Biomass-based carbon materials for CO_2 capture: A review. *Journal of CO_2 Utilization* 2023; **68**, 102373.

[42] M Burachevskaya, T Minkina, T Bauer, I Lobzenko, A Fedorenko, M Mazarji, S Sushkova, S Mandzhieva, A Nazarenko, V Butova, MH Wong and VD Rajput. Fabrication of biochar derived from different types of feedstocks as an efficient adsorbent for soil heavy metal removal. *Scientific Reports* 2023; **13**, 2020.

[43] NK Achmelwar, SB Sollapur, YA Kharche and SGG Devakant. Processing and characterization of germanium-based borate bioglass for biological applications. *Engineering Reports* 2025, **7(7)**, e70253.

[44] J Serafin, B Dziejarski, ÓJ Fonseca-Bermúdez, L Giraldo, R Sierra-Ramírez, MG Bonillo, G Farid and JC Moreno-Piraján. Bioorganic activated carbon from cashew nut shells for H_2 adsorption and industrial applications. *International Journal of Hydrogen Energy* 2024; **86**, 662-676.

[45] N Chaiammart, V Vignesh, MM Thu, A Eiad-ua, T Maiyalagan and G Panomsuwan. Chemically activated carbons derived from cashew nut shells as potential electrode materials for electrochemical supercapacitors. *Carbon Resources Conversion* 2025; **8(2)**, 100267.

[46] SY Yang, BC Bai and YR Kim. Effective surface structure changes and characteristics of activated carbon with the simple introduction of oxygen

functional groups by using radiation energy. *Surfaces* 2024; **7(1)**, 12-25.

[47] X Song, J Gong, X Zhan and Y Zeng. Exploring a new method to study the effects of surface functional groups on adsorption of CO_2 and CH_4 on activated carbons. *Langmuir* 2020; **36(14)**, 3862-3870.

[48] D Shrestha. Structural and electrochemical evaluation of renewable carbons and their composites on different carbonization temperatures for supercapacitor applications. *Heliyon* 2024; **10**, e25628.

[49] N Czerwinska, C Giosu, I Matos, S Sabbatini, L Ruello and M Bernardo. Development of activated carbons derived from wastes: coffee grounds and olive stones as potential porous materials for air depollution. *Science of the Total Environment* 2024; **914**, 169898.

[50] M. Thommes. Physical adsorption characterization of nanoporous materials. *Chemie Ingenieur Technik* 2010; **82(7)**, 1059-1073.

[51] S Ha, SG Jeong, S Myeong, C Lim and Y Lee. High-performance CO_2 adsorption of jellyfish-based activated carbon with many micropores and various heteroatoms. *Journal of CO_2 Utilization* 2023; **76**, 102589.

[52] B Sun, Q Yang, J Zhu, T Shao, Y Yang, C Hou and G Li. Pore size distributions and pore multifractal characteristics of medium and low-rank coals. *Scientific Reports* 2020; **10(1)**, 22353.

[53] D Peredo-Mancilla, A Bermudez, C Hort and D Bessieres. Surface-modified activated carbon with a superior CH_4 /CO_2 adsorption selectivity for the biogas upgrading process. *Industrial & Engineering Chemistry Research* 2022; **61**, 12710-12727.

[54] D Peredo-Mancilla, A Bermudez, C Hort and D Bessieres. Exploring activated carbons for sustainable biogas upgrading: A Comprehensive Review. *Energies* 2025; **18**, 4010.

[55] C Quan, H Wang, X Jia and N Gao. Effect of carbonization temperature on CO_2 adsorption behavior of activated coal char. *Journal of the Energy Institute* 2021; **97**, 92-99.

[56] M Vashishtha, S Gadipelli and KV Kuma. Deliverable capacity of methane: Required material property levels for the ideal 'Holy Grail' adsorbent. *Chem & Bio Engineering* 2025; **2(1)**, 64-67.